Noncollinear full-potential studies of γ-Fe

Elisabeth Sjöstedt and Lars Nordström
Condensed Matter Theory Group, Physics Department, Uppsala University, S-75121 Uppsala, Sweden
(Received 17 January 2002; published 24 July 2002)

Accurate density functional calculations have been performed for the fcc-based frustrated antiferromagnet γ-Fe. Several competing collinear as well as noncollinear magnetic structures have been considered: ferromagnetism, $1\mathbf{k}$, $2\mathbf{k}$, $3\mathbf{k}$, and double-layered antiferromagnetism, as well as noncommensurate helices. In contrast to standard noncollinear methods, our scheme treats the magnetization density as a vector field which is free to change in both magnitude and direction throughout space. The noncollinear method is implemented in the alternative linearization of the full-potential augmented-plane-wave method, closely related to the conventionally linearized method, but computationally more efficient. The most stable magnetic structure of γ-Fe is found to vary sensitively with volume. At the experimental volume $a=6.82$ a.u., the moments are ordered in a collinear double-layered antiferromagnetic structure, while the ground state is almost degenerate between two different helices of different equilibrium volumes $a=6.63$ a.u. and $a=6.61$ a.u., respectively. The obtained results are analyzed and compared with earlier calculations and existing experiments. For instance, we notice that the results are altered when we introduce an atomic moment approximation in our calculations.

DOI: 10.1103/PhysRevB.66.014447 PACS number(s): 75.25.+z, 71.15.Mb

I. INTRODUCTION

The high-temperature fcc phase of iron, γ-Fe, has attracted much interest due to its elusive magnetic character. There are also practical implications since many important iron alloys, such as the Invar alloys and several high-quality stainless steels, are fcc ordered.

In 1989 Tsunoda[1] managed to stabilize precipitates of γ-Fe inside an fcc Cu matrix. They could then explore the magnetic properties of three-dimensionally constrained clusters of γ-Fe, each one spherically shaped with a mean diameter of 50 nm. Interestingly enough, the ground state was found to be a helical spin density wave, or a spin spiral (SS), with a wave vector

$$\mathbf{q}_{expt}=(0.10,0,1)\frac{2\pi}{a}. \tag{1}$$

Here a is the lattice constant of the conventional fcc Cu cell (6.822 a.u.), inherited by the iron precipitates. This wave vector nearly yields a type-I antiferromagnetic (AF) system, cf. $\mathbf{q}_{AF}=(0,0,1)2\pi/a$.

From a theoretical point it is unclear what magnetic ground state γ-Fe is predicted to have, since there is an unusual large spread in earlier published results. The first spin-spiral calculations performed for γ-Fe were presented by Mryasov *et al.*[2] in 1991. Using the linearized muffin-tin orbital (LMTO) method they investigated ordering vectors in the $\Gamma\widetilde{X}$ direction of the fcc Brillouin zone (BZ), where the $\mathbf{q}$ vector Γ is equivalent to a ferromagnetic (FM) structure, and the ordering vector X represents a type-I AF structure. They found that the magnetic ground state depends on the filling of $3d$ electrons, with γ-Fe lying at a crossing point between the FM and AF regions in a magnetic phase diagram of $3d$ metals in fcc lattices. They also showed how the magnetic structure of γ-Fe could be changed from FM into different SS structures by lowering the lattice parameter from 7.11 a.u. down to 6.81 a.u. For the smaller volumes, the energy of the SS approached that of the AF solution. The lowest energy was found for the smallest volume examined, at a SS having $\mathbf{q}$ vector

$$\mathbf{q}_A=(0,0,0.6)\frac{2\pi}{a}. \tag{2}$$

The same ordering vector was obtained in the calculations performed by Uhl *et al.*[3] later the same year. They used the augmented spherical wave (ASW) method and included also $\mathbf{q}$ vectors along $\widetilde{XW}$. Antropov *et al.*[4] let the directions of the magnetic moments evolve freely in an LMTO calculation, using a supercell with 32 atoms. They confirmed that the magnetic configuration was extremely sensitive to volume changes. Their results changed quantitatively when the local spin density approximation (LSDA) was replaced by a generalized gradient approximation (GGA) but the trend was the same, going from more complex orderings at small volumes ($a<6.78$ a.u. and $a<6.69$ a.u. for the LSDA and GGA, respectively) into a double-layered AF structure for increasing volumes. For larger volumes ($a>7.05$ and $a>6.90$ a.u.), the structure preferred the FM state. James *et al.*[5] performed LMTO calculations where they compared the total energy as function of the volume for a large number of AF orderings in γ-Fe. Using the LSDA they found a more complex ordering of the moments at smaller volumes $a<6.78$ a.u., with the global minimum at $a=6.55$ a.u. Again, the double-layered AF structure became the most stable for increasing volumes.

In their paper from 1996, Körling and Ergon[6] reproduced the SS structure of ordering vector $\mathbf{q}_A$ for a lattice constant $a=6.80$ a.u. using the LMTO method with LSDA. However, when introducing the GGA into their calculations, they stabilized a new SS with an ordering vector at W,

$$\mathbf{q}_B=(0.5,0,1)\frac{2\pi}{a}. \tag{3}$$

This **q** vector is not in agreement with $\mathbf{q}_{expt}$, but nevertheless it showed that the GGA had a large effect on their results.

All the calculations above have in common that they represented their potential using the atomic sphere approximation (ASA). However, Körling and Ergon[6] showed how their collinear LMTO-ASA magnetization energies were overestimated compared to full-potential linearized augmented-plane-wave (FLAPW) calculations. The magnitude of this overestimation was comparable to the relative stabilization energy between the lowest-lying SS and the AF solutions of the LMTO-ASA.

This result pointed out the demand for more exact noncollinear calculations for determining the most stable structures in fcc Fe, and subsequently a few non-ASA calculations have been presented. First, Herper *et al.*[7] compare three collinear orderings in their energy versus volume curve: the FM, the type-I AF, and the double-layered AF orderings. Using the FLAPW method and GGA, they find the AF and double-layered AF structures to form almost degenerate ground states, with equilibrium lattice constants of $a=6.60$ a.u. and $a=6.68$ a.u., respectively.

The ultrasoft pseudopotential calculations allowing for a noncollinear spin spiral by Bylander and Kleinman[8] showed no drastic changes from the corresponding ASA calculations, yielding a stable SS state with ordering vector close to $\mathbf{q}_A$,

$$\mathbf{q}=(0,0,0.55)\frac{2\pi}{a}. \tag{4}$$

What instead altered the energy versus ordering vector curve was their GGA implementation.[9] This calculation gave, however, a larger energy for $\mathbf{q}=X$ than for $\mathbf{q}=\Gamma$, in contradiction with earlier collinear calculations as well as all noncollinear calculations. The most stable ordering vector was, however, still that of Eq. (4). In order to correct for some known deficiencies of the GGA, they added an *ad hoc* ''spin-stiffness correction''[10] to the GGA, which changed the shape of their energy curve drastically, now with the global minimum at $\mathbf{q}=X$.

In a recent paper Knöpfle *et al.*,[11] presented a *modified* ASW method (MASW), in order to take care of some full potential effects beyond the ASA approximation. For lattice constants $a\leqslant 6.75$ a.u. the modified method gives a new ground-state **q** vector

$$\mathbf{q}_C=(0.15,0,1)\frac{2\pi}{a}, \tag{5}$$

which agrees well with experiments, although for somewhat smaller lattice constants. Their results are not altered drastically either by the introduction of the GGA or by turning off the intra-atomic noncollinear magnetism introduced in this method. Thus, the stabilization of this new ordering vector must be understood as due to the the full potential (FP) corrections to the atomic sphere approximation. Kurz *et al.*[12] used γ-Fe with $a=6.70$ a.u. as a trial system in their presentation of different implementations of the GGA in the LAPW method. Going beyond the ASA, but still using a kind of atomic moment approximation (see Sec. II for a definition) they find the most stable SS to have an ordering vector equal to $\mathbf{q}_A$. The aim of the present paper is, inspired by the different results and contradictions found when reviewing previous results, to investigate the theoretical ground state of γ-Fe using the highly precise alternative linearization of the FLAPW (FP-APW+lo) method within the GGA. The magnetization density is represented by a field quantity everywhere in the unit cell, in order to make the calculations as accurate as possible.

The paper is organized as follows. The scheme used to describe noncollinearity is presented in Sec. II. Although this method has been used before,[13–15] it has never been properly described, so we take the opportunity to discuss its implementation in some details. Section III holds the results in the form of total energies and magnetic moments of the various magnetic structures. The discussion and conclusions are presented in Secs. IV and V.

II. METHOD

Since the pioneering work a decade ago,[16,17] quite a few density-functional-based electronic structure calculations have been reported which have allowed for noncollinear magnetism (NCM). However, a majority of the calculations up to present day have in common that they have assumed that the noncollinearity is on an interatomic scale; i.e., each atom has a single spin-quantization axis and the magnetization density is locally collinear within the region of an atom. Although this approximation with a locally collinear atomic moment, which we will refer to as an atomic moment approximation (AMA), is a fast and convenient approximation, it is by no means enforced by the LSDA (Ref. 18) to the density functional theory.

We will here describe how a general implementation of the LSDA, with no shape or directional approximations for the magnetization density (Fig. 1), can be implemented in a full-potential method.

First, a short review of the general noncollinear version of the LSDA will be given together with a discussion of gradient corrections. Then we will describe how this scheme can be implemented in the presently used full-potential linear augmented-plane-wave (FP-APW+lo) (Ref. 19) method. Especially, details of the implementation of the noncommensurate helical spin wave, which is often referred to as a spin spiral, will be discussed.

A. Noncollinear local spin density approximation

When generalizing density functional theory (DFT) (Refs. 20 and 21) to a spin-dependent theory, von Barth and Hedin[18] introduced a 2×2 density matrix $\rho(\mathbf{r})$ which generally can be expanded as $\rho=(n\mathcal{I}+\mathbf{m}\cdot\boldsymbol{\sigma})/2$, where $\mathcal{I}$ is the 2×2 unit matrix and $\boldsymbol{\sigma}=(\sigma_x,\sigma_y,\sigma_z)$ are the Pauli spin matrices. The new physical quantity, besides the charge density *n*, is the magnetization density $\mathbf{m}(\mathbf{r})$ which naturally is a vector density.

The effective one-electron potential, which is defined through functional derivatives of the total energy functional with respect to the density,[18,21] also becomes a 2×2 matrix,

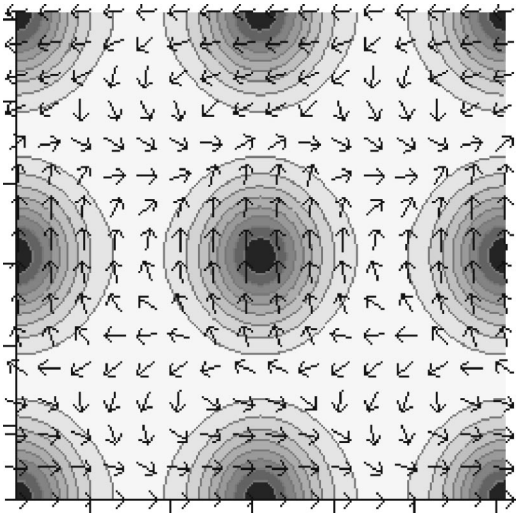

FIG. 1. The magnetization density of the $\mathbf{q}_1$ SS, shown in the xz plane of the conventional fcc cell. The y coordinate is fixed at $a/4$ for $a=6.63$ a.u.; thus, the corner atoms, along with the center atom, lie $a/4$ out from the paper, while the atom on the middle of each side lies $a/4$ into the paper. The magnetization density is treated as a vector field; i.e., it is free to change both in magnitude and direction throughout space. The gray scale shows different magnitudes of the moments, with darker shades corresponding to larger moments, and the noncollinear directions are indicated by unit vectors.

$V(\mathbf{r})=v(\mathbf{r})\mathcal{I}-\mathbf{b}(\mathbf{r})\cdot\boldsymbol{\sigma}$. The nonmagnetic part $v(\mathbf{r})$ includes, besides the exchange-correlation potential, the nuclei attraction and the Hartree term, while the magnetic part $\mathbf{b}(\mathbf{r})$ of the potential matrix only has contributions from the exchange-correlation functional. Since we are here interested in the magnetic contributions, we will focus on the exchange-correlation terms.

In the LSDA the exchange-correlation functional is given by[18]

$$E_{\mathrm{xc}}[n(\mathbf{r}),\mathbf{m}(\mathbf{r})]=\int n(\mathbf{r})\varepsilon_{\mathrm{xc}}(n(\mathbf{r}),|\mathbf{m}(\mathbf{r})|)d\mathbf{r}, \tag{6}$$

where $\varepsilon_{\mathrm{xc}}(n,m)$ is the exchange-correlation energy density for a spin-polarized homogeneous electron gas with charge density n and magnetization density of magnitude m. The actual functional form of $\varepsilon_{\mathrm{xc}}(n,m)$ which has been parametrized in various different ways[18,22,23] has no importance for our general discussion. The LSDA exchange-correlation functional leads to the nonmagnetic scalar exchange-correlation potential

$$\begin{aligned}v_{\mathrm{xc}}(\mathbf{r})&=\frac{\delta E_{\mathrm{xc}}}{\delta n(\mathbf{r})}\\&=\varepsilon_{\mathrm{xc}}(n(\mathbf{r}),|\mathbf{m}(\mathbf{r})|)+n(\mathbf{r})\left[\frac{\partial\varepsilon_{\mathrm{xc}}(n,m)}{\partial n}\right]_{n=n(\mathbf{r}),m=|\mathbf{m}(\mathbf{r})|}\end{aligned} \tag{7}$$

and to the magnetic potential, which is in the form of a magnetic field,

$$\begin{aligned}\mathbf{b}(\mathbf{r})&=-\frac{\delta E_{\mathrm{xc}}}{\delta\mathbf{m}(\mathbf{r})}=-\frac{\delta|\mathbf{m}(\mathbf{r})|}{\delta\mathbf{m}(\mathbf{r})}\frac{\delta E_{\mathrm{xc}}}{\delta|\mathbf{m}(\mathbf{r})|}\\&=-\hat{\mathbf{m}}(\mathbf{r})n(\mathbf{r})\left[\frac{\partial\varepsilon_{\mathrm{xc}}(n,m)}{\partial m}\right]_{n=n(\mathbf{r}),m=|\mathbf{m}(\mathbf{r})|},\end{aligned} \tag{8}$$

where $\hat{\mathbf{m}}(\mathbf{r})=\delta|\mathbf{m}(\mathbf{r})|/\delta\mathbf{m}(\mathbf{r})$ is the direction of the magnetization density at the point $\mathbf{r}$. As is clear from Eq. (8), the potential $\mathbf{b}$ is collinear to the magnetization density $\mathbf{m}$ everywhere.

Although the potential of Eq. (8) is obtained within the LSDA, we would like to stress the difference to the usual enforced collinear adaptation, where the spin magnetization density enters as a scalar quantity.

In contrast to the local approximation there exists no formulation for a noncollinear gradient corrected approximation (GGA).[24,25] This is because the assumption of a collinear spin magnetization leads to only one gradient, while a general formulation requires three, one for each component. When generalizing existing GGA schemes to the noncollinear case, one can choose whether the sole magnetization gradient refers to the gradient of the magnitude of the magnetization density or the gradient of the component locally parallel to the magnetization density. In practice, this choice has little importance,[12] and we have chosen the latter, the longitudinal gradient, approach. However, for consistency a true noncollinear GGA should be formulated, which would include the effect of the gradient of the transversal components too. In the absence of this effect, the exchange-correlation magnetic field falls out to be locally parallel to the magnetization density, as in the LSDA. There have been suggestions for improving upon the existing GGA deficiency, either by introducing an *ad hoc* spin stiffness term[10] or by deriving the GGA from current density formalism.[26]

The spin-dependent Kohn-Sham[21] Hamiltonian becomes

$$\mathcal{H}=-\mathcal{I}\nabla^2+V(\mathbf{r})=\{-\nabla^2+v(\mathbf{r})\}\mathcal{I}-\mathbf{b}(\mathbf{r})\cdot\boldsymbol{\sigma}. \tag{9}$$

If the eigenfunctions ψ_i of this Hamiltonian are written in spinor form, the magnetization and charge densities can be directly constructed by summing over the occupied states,

$$\mathbf{m}(\mathbf{r})=\sum_i^{\mathrm{occ}}\psi_i^\dagger(\mathbf{r})\boldsymbol{\sigma}\psi_i(\mathbf{r}) \quad\text{and}\quad n(\mathbf{r})=\sum_i^{\mathrm{occ}}\psi_i^\dagger(\mathbf{r})\psi_i(\mathbf{r}), \tag{10}$$

which readily allow for the usual iterative solution. A self-consistent solution is obtained when the input charge and magnetization density produce the same output charge and magnetization density; i.e., also the noncollinearity of the magnetization density is given by this self-consistency procedure.

The expression for the total energy looks like

$$\begin{aligned}E=&\sum_i^{\mathrm{occ}}\varepsilon_i-\frac{1}{2}\int n(\mathbf{r})v_{\mathrm{C}}(\mathbf{r})d\mathbf{r}\\&-\int[n(\mathbf{r})\{v_{\mathrm{xc}}(\mathbf{r})-\varepsilon_{\mathrm{xc}}(\mathbf{r})\}-\mathbf{m}(\mathbf{r})\cdot\mathbf{b}(\mathbf{r})]d\mathbf{r},\end{aligned} \tag{11}$$

where ε_i are the eigenenergies and v_C is the classical Coulomb part of the spin-independent potential, i.e., the Hartree and nuclei contributions.

Collinear magnetism can easily be seen to be the special case with the magnetization density parallel to a global direction, say, $\hat{\mathbf{e}}$. In this case, it is possible to define global spin-up and spin-down potentials $v^{\pm}=v\mp\mathbf{b}\cdot\hat{\mathbf{e}}$, and the Hamiltonian (9) may be transformed into a block diagonal form

$$\mathcal{H}'=U\mathcal{H}U^{\dagger}=\begin{pmatrix}-\nabla^2+v^{+}(\mathbf{r}) & 0\\ 0 & -\nabla^2+v^{-}(\mathbf{r})\end{pmatrix}, \quad (12)$$

where U is the spin-1/2 rotation matrix for a rotation of the spin-quantization axis, from $\hat{\mathbf{z}}$ to $\hat{\mathbf{e}}$. The eigenspinors in this representation are of pure spin-up or spin-down character, which will provide that the output magnetization density will be collinear, with the global direction $\hat{\mathbf{e}}$. However, it should be noted that when spin-orbit coupling is included in the Kohn-Sham Hamiltonian a truly collinear solution is actually *never possible*, since the spin-orbit coupling term always gives arise to some nontrivial spin mixture in the eigenspinors.[13]

As discussed above, a common approach to NCM is to approximate this magnetization density, continuous both in direction and magnitude, by one where the direction is defined on a coarse mesh, i.e., with different local spin quantization axes for different atoms. This is what we already have denoted AMA and corresponds to substituting $\hat{\mathbf{m}}$ by

$$\hat{\mathbf{m}}_{\mathrm{AMA}}(\mathbf{r})=\hat{\mathbf{e}}_{\alpha} \text{ for } \mathbf{r}\in \text{ atom } \alpha, \quad (13)$$

and $|\mathbf{m}|\equiv\hat{\mathbf{m}}\cdot\mathbf{m}$ by $\hat{\mathbf{m}}_{\mathrm{AMA}}\cdot\mathbf{m}$ in Eq. (8). Here $\hat{\mathbf{e}}_{\alpha}$ is the direction of the local spin-quantization axis of atom α, which is parallel to the local moment of the atom $\langle\mathbf{m}\rangle_{\alpha}=\int_{\alpha}\mathbf{m}\,d\mathbf{r}$. This means that the magnetic potential is locally parallel to the atomic moment, which is why we have given this approach its name.[27] The partitioning of space into atomic regions is of course somewhat arbitrary and may vary between different calculations.

It should also be noted that in AMA approaches, the four quantities used to describe the 2×2 density matrix are often taken to be n, $m=|\mathbf{m}|$, θ, and φ, where θ and φ are the polar angles which describes the direction of $\hat{\mathbf{m}}$ or, equivalently, $\hat{\mathbf{e}}_{\alpha}$. However, in the present case, where we need a continuous description, these angles are not well suited, because of the presumptive jumps by 2π and the nondefined values of φ when $\theta=0$ or π. Since it is crucial that the relevant quantities are continuous and easy to Fourier transform, we instead prefer to work with n and the three Cartesian components of $\mathbf{m}$.

B. Implementation into the FP-APW+lo method

We implemented this noncollinear LSDA,[13] to our knowledge for the first time in its general form, in the full-potential linear augmented plane-wave method. The method we use (FP-APW+lo) (Ref. 19), differs from the traditional full-potential linearized-augmented-wave method (Refs. 28 and 29) in the way the plane-wave basis functions are augmented and has proved to be more efficient. The FLAPW and FP-APW+lo methods are, however, closely related, and the following description of the noncollinear LSDA implementation into the FP-APW+lo method can equally well be used for the FLAPW method.

In the augmented-plane-wave method the space is divided into two regions: nonoverlapping spheres centered at each atom, so-called muffin-tin (MT) spheres, and the rest—the interstitial (I). In the interstitial the basis set consists of plane waves, while in the muffin tins these plane waves are augmented by a spherical expansion of radial functions, i.e.,

$$\chi_j(\mathbf{k},\mathbf{r})=\begin{cases}\Omega^{-1/2}e^{i(\mathbf{k}+\mathbf{G}_j)\cdot\mathbf{r}}, & \mathbf{r}\in\mathrm{I},\\ \sum_{\alpha L} f_{j\alpha L}(r_{\alpha})Y_L(\hat{\mathbf{r}}_{\alpha}), & \mathbf{r}\in\mathrm{MT},\end{cases} \quad (14)$$

where $\mathbf{k}$ is a wave vector in the Brillouin zone, $\mathbf{G}_j$ is the reciprocal lattice vector of the plane wave, Y_L are spherical harmonics, $L=\{lm\}$ is the angular momentum index, Ω is the volume of the unit cell, and $\mathbf{r}_{\alpha}=\mathbf{r}-\mathbf{R}_{\alpha}$ is the muffin-tin centered coordinate of atom α.

The radial functions inside the muffin-tin sphere of atom α are expanded using MT orbitals $\phi_{\nu\alpha l}$, which solve the radial Schrödinger equation

$$\left\{-\frac{d^2}{dr^2}+\frac{l(l+1)}{r^2}+v_{\alpha}(r)-\varepsilon_{\nu\alpha l}\right\}r\phi_{\nu\alpha l}(r)=0. \quad (15)$$

Since $v_{\alpha}(r)$ is the spherical part of the actual potential, these functions are capable of giving a good description of the local wave function for energies around the linearization energy $\varepsilon_{\nu\alpha l}$. This expansion can be performed in different ways. The traditional FLAPW method uses a linear combination of $\phi_{\nu\alpha l}$ and their energy derivatives $\dot{\phi}_{\nu\alpha l}$, which gives continuous and differentiable basis functions at the sphere boundary. In the FP-APW+lo method, the corresponding augmentation is simply $f_{j\alpha L}(r)=a_{j\alpha L}\phi_{\nu\alpha l}(r)$. These basis functions, Eq. (14), are then complemented by a set of local orbitals,[29,30]

$$\chi_j(\mathbf{k},\mathbf{r})=\begin{cases}0 & \mathbf{r}\in\mathrm{I},\\ g_{j\alpha L}(r_{\alpha})Y_L(\hat{\mathbf{r}}_{\alpha}) & \mathbf{r}\in\mathrm{MT},\end{cases} \quad (16)$$

where $g_{j\alpha L}(r)=\phi_{\nu\alpha l}(r)+b_{j\alpha L}\dot{\phi}_{\nu\alpha l}(r)$. Thus, each local orbit j has a specific αL character and is independent of the wave vector $\mathbf{k}$. The two expansion coefficients a and b are fixed by the criterion that the basis functions should be continuous at the sphere boundary. For the plane wave basis functions the analytical expressions is found by using the well-known expansion of a plane wave in spherical Bessel functions.

In most spin-polarized versions of the augmented plane-wave method, there are spin-up and spin-down versions of ϕ and $\dot{\phi}$ which are the solutions of Eq. (15) with the local spherical spin-up and spin-down potentials, respectively. In the present implementation we have chosen to use a spin-

independent basis, and v_α is taken to be the spherical average of the nonmagnetic potential v around atom α. This drastically simplifies the augmentation at the sphere boundary, since now *the basis set* never involves globally spin-mixed spinors. In cases of strong exchange splitting the loss of flexibillity of this spin-independent basis set inside the MT spheres can be more than compensated by an extention of the the basis set, Eqs. (14) and (16), with another type of local orbitals[30] where the energy derivative of ϕ is replaced by a second radial function, so that

$$g_{j\alpha L}(r)=\phi_{\nu\alpha l}(r)+c_{j\alpha L}\phi_{\mu\alpha l}(r). \tag{17}$$

This new function $\phi_{\mu\alpha l}$ is the solution of Eq. (15) for a linearization energy $\varepsilon_{\mu\alpha l}\neq\varepsilon_{\nu\alpha l}$. The coefficient c is set so that the value of the local orbital matches zero at the sphere boundary. The inclusion of extra local orbitals leads to a rather small increase in the number N of spin-independent basis functions χ_j, while $\phi_{\mu\alpha l}$ provides an increased flexibility to the wave functions within the MT spheres. We have performed tests for the ferromagnetic $3d$ metals and verified that such a spin-independent basis reproduces the ordinary collinear spin-dependent basis set results.

The generalized eigenvalue problem at the wave vector $\mathbf{k}$ is of the order $2N\times 2N$ and has, with our choice of spin-independent basis functions, the form

$$[\{\mathcal{H}(\mathbf{k})-\varepsilon_i\mathcal{O}(\mathbf{k})\}\mathcal{I}-\mathbf{B}(\mathbf{k})\cdot\boldsymbol{\sigma}]\mathbf{c}_i=0, \tag{18}$$

where ε_i is the ith eigenvalue and $\mathbf{c}_i$ is the corresponding eigenvector. $\mathcal{O}$ is the $N\times N$ overlap matrix

$$\mathcal{O}_{ij}(\mathbf{k})=\int \chi_i^*(\mathbf{k},\mathbf{r})\chi_j(\mathbf{k},\mathbf{r})d\mathbf{r}, \tag{19}$$

and $\mathcal{H}$ is the $N\times N$ nonmagnetic Hamiltonian matrix

$$\mathcal{H}_{ij}(\mathbf{k})=\int \chi_i^*(\mathbf{k},\mathbf{r})\{-\nabla^2+v(\mathbf{r})\}\chi_j(\mathbf{k},\mathbf{r})d\mathbf{r}. \tag{20}$$

They are identical to the matrices which would enter a non-spin-polarized calculation with a potential equal the nonmagnetic potential. The magnetic potential enters through the $N\times N$ matrices $\mathbf{B}$:

$$\mathbf{B}_{ij}(\mathbf{k})=\int \chi_i^*(\mathbf{k},\mathbf{r})\mathbf{b}(\mathbf{r})\chi_j(\mathbf{k},\mathbf{r})d\mathbf{r}. \tag{21}$$

These matrix elements are evaluated independently for the three components by expanding the potential in the usual way[29] in terms of plane waves in the interstitial and spherical harmonics within the MT spheres—and performing the resulting integrals. The $2N$ eigenspinors that are obtained after the matrix diagonalization are of the form

$$\psi_i(\mathbf{k},\mathbf{r})=\sum_j^N \mathbf{c}_{i,j}\chi_j(\mathbf{k},\mathbf{r})=\sum_j^N \begin{pmatrix}\alpha_{i,j}\\ \beta_{i,j}\end{pmatrix}\chi_j(\mathbf{k},\mathbf{r}), \tag{22}$$

i.e., with the spin dependence entering through the coefficients $\mathbf{c}=(\alpha,\beta)^T$. The charge density and the three components of the magnetization density are independently constructed according to Eq. (10) and subsequently expanded in plane waves and spherical harmonics.

Since the LSDA exchange-correlation potential, due to its nonlinear dependence on the local densities, preferably is evaluated in real space, there are not much extra effort in evaluating the general magnetic potential of Eq. (8) in comparison with a collinear one. Neither in the total energy calculations does the exchange-correlation contribution cause any extra work. This stems from the fact that the total energy is usually, for sake of convenience, evaluated using the input densities, which means that **m** and **b** are parallel in Eq. (11). As FP-APW+lo is an all-electron method the core states are recalculated in each iteration step. However, here we do restrict ourselves to the AMA for the spin-polarized potential. This should have very little, if any, influence on the calculations, especially when properties influenced by the core electrons, e.g., hyperfine fields, are not in focus.

C. Spin-spiral symmetry

The above formalism is valid for cases where the magnetic unit cell is identical to the unit cell used in the calculation. However, it was shown by Herring[31] that if spin space can be decoupled from the lattice, i.e., when the relativistic spin-orbit coupling can be neglected, noncommensurate helical or cyclic waves can be treated with a unit cell governed by the chemical rather than the magnetic symmetry. These systems are often referred to as spin spirals. Sandratskii and Guletskii have discussed how to implement them into DFT methods.[17] Here we will discuss mainly how to generalize this technique, developed for AMA methods, to the case of a full-potential method.

A spin spiral with wave vector $\mathbf{q}$ is defined by its translational properties,

$$\mathcal{T}\mathbf{m}(\mathbf{r})=\mathbf{m}(\mathbf{r}+\mathbf{R})=\mathcal{R}(\mathbf{q}\cdot\mathbf{R})\mathbf{m}(\mathbf{r}), \tag{23}$$

where $\mathcal{R}(\phi)$ is a rotation by the angle $\phi=\mathbf{q}\cdot\mathbf{R}$ around a given axis and $\mathbf{R}$ is any lattice vector. Since spin and space are not coupled, we have the freedom to take this axis to be parallel to $\mathbf{q}$ in space and parallel to z in spin space. Hence, the two components perpendicular to this axis (i.e., x and y components) continuously rotate when the spiral propagate along $\mathbf{q}$. When the z component is identical zero, we refer to the spiral as planar, otherwise as conical.

Now one can introduce some generalized translation operators $\mathcal{T}_\mathcal{R}=\mathcal{R}^{-1}\mathcal{T}$, under which the spin-spiral magnetization density is an invariant, $\mathcal{T}_\mathcal{R}\mathbf{m}=\mathbf{m}$. As the exchange-correlation field is everywhere parallel to the magnetization density, both in the LSDA and in the present version of the GGA, this is also true for the magnetic field **b**.

In the present implementation into a method which uses plane-wave representations of densities and potentials, these quantities ought to be translationally invariant with the periodicity of the chemical unit cell in order to efficiently make use of fast Fourier transforms. Hence, we have to take a slightly different route compared to previous formulations, which were more suitable to methods using local representations of the basis.[17] First, new complex quantities u and h are

introduced, which represent the rotations of the two components perpendicular to the spin spiral axis,

$$u(\mathbf{r}) = e^{-i\mathbf{q}\cdot\mathbf{r}}\{m_x(\mathbf{r}) + i m_y(\mathbf{r})\} \tag{24}$$

and

$$h(\mathbf{r}) = e^{-i\mathbf{q}\cdot\mathbf{r}}\{b_x(\mathbf{r}) + i b_y(\mathbf{r})\}. \tag{25}$$

These new densities are translationally invariant by construction, e.g., $\mathcal{T}u = u$. Further, following from the parallelism of m and b, they are *parallel*, so that $\arg u = \arg h$.

The Kohn-Sham Hamiltonian now becomes

$$\mathcal{H} = \{-\nabla^2 + v(\mathbf{r})\}\mathcal{I} - \{e^{i\mathbf{q}\cdot\mathbf{r}} h(\mathbf{r})\boldsymbol{\sigma}_- + \text{H.c.}\} - b_z(\mathbf{r})\boldsymbol{\sigma}_z, \tag{26}$$

where $\sigma_- = \frac{1}{2}(\sigma_x - i\sigma_y)$.

It was shown by Herring[31] that $\mathcal{H}$ is diagonalized by the generalized Bloch spinors

$$\psi_{j,\mathbf{k}}(\mathbf{r}) = \begin{pmatrix} e^{i(\mathbf{k}-\mathbf{q}/2)\cdot\mathbf{r}}\alpha_{j,\mathbf{k}}(\mathbf{r}) \\ e^{i(\mathbf{k}+\mathbf{q}/2)\cdot\mathbf{r}}\beta_{j,\mathbf{k}}(\mathbf{r}) \end{pmatrix}, \tag{27}$$

where α and β are translationally invariant functions, from which we construct the new densities, especially,

$$u(\mathbf{r}) = \sum_{j,\mathbf{k}}^{\text{occ}} \psi^\dagger_{j,\mathbf{k}}\{e^{-i\mathbf{q}\cdot\mathbf{r}} 2\sigma_+\}\psi_{j,\mathbf{k}}. \tag{28}$$

III. RESULTS

The calculations presented in this section are performed using the full-potential linearized augmented-plane-wave method (FP-APW+lo) (Ref. 19) with the GGA correction as described in Sec. II A. In addition to the different spin spiral structures, we examine the noncollinear $2\mathbf{k}$ and $3\mathbf{k}$ orderings, and finally the collinear double-layered antiferromagnetic structure.

A. Calculational details

All calculations are converged in $\boldsymbol{k}$ points as well as in number of basis functions. The BZ integration is performed by means of special $\mathbf{k}$ points, around 4000 $\mathbf{k}$ points in the first BZ, together with a temperature broadening of $k_BT = 5$ mRy. The plane-wave cutoff is set to $K_{max} = 4.9$ a.u.$^{-1}$, except for the double-layered AF structure where $K_{max} = 4.4$ a.u.$^{-1}$, and the augmentation is performed for angular momentum $l \leq 9$. The two kinds of local orbitals, Eqs. (16) and (17), are used for $l = s$, p, and d throughout. The MT sphere is treated using a logarithmic radial mesh of 1450 steps, from $\mathbf{r}_0 = 1.15 \times 10^{-6}$ a.u., to the muffin tin radius $\mathbf{r}_{MT} = 2.25$ a.u. Non-MT contributions are added to the last 300 mesh points. This particular mesh was found to be converged in number of mesh points. Smaller meshes were found to give unreliable results, especially for the spin-spiral calculations.

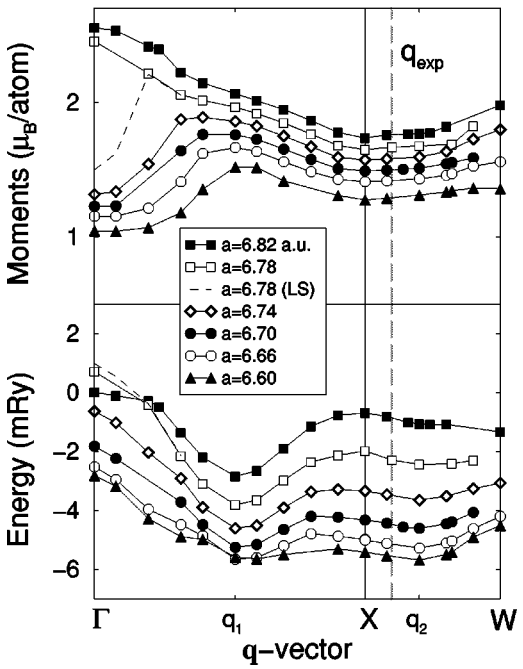

FIG. 2. The upper and lower panels show the moments and the total energy, respectively, as a function of the spin-spiral wave vector. Each curve represents a volume corresponding to lattice constants $6.60 \leq a \leq 6.82$ a.u. The experimental wave vector is shown as the vertical dashed line. Two stable spin spirals are found, indicated as $\mathbf{q}_1$ and $\mathbf{q}_2$. The total energies are given relative to the FM structure at $a = 6.82$ a.u.

B. Spin spirals

The first magnetic structures examined are the spin spiral states for $\mathbf{q}$ vectors along the symmetry lines $\overrightarrow{\Gamma X}$ and $\overrightarrow{XW}$ of the fcc BZ. Starting from the lattice constant of copper, $a = 6.82$ a.u., the volumes are successively decreased in order to determine the equilibrium volume. The lower panel of Fig. 2 shows how the total energy varies with $\mathbf{q}$ for different fcc lattice constants. At large volumes, the most stable spin-spiral structure is found to have an ordering vector

$$\mathbf{q}_1 = (0,0,q)\frac{2\pi}{a}, \tag{29}$$

where q changes with volume from 0.53 to 0.59; see Table I. This energy minimum exists for all volumes considered, and the energy of this spin-spiral structure stays around 3 mRy lower than the corresponding FM energy, while the energy difference between the SS and the AF state decreases with volume.

The magnitude of the magnetic moments $\langle \mathbf{m} \rangle$, in the upper panel of Fig. 2, is found through integration of the magnetic moment vector field over the muffin-tin sphere. Here one can clearly observe the crossover from a FM high-spin (HS) state to a FM low-spin (LS) state that occurs at a lattice constant just below $a = 6.78$ a.u. This crossover exists only at the center of the BZ. Further out in the BZ, e.g., for $\mathbf{q}_1$, the decrease of the magnetic moments is continuous. So for the FM state we observe moments in the range $(1.0–2.5)\mu_B$, while the AF moments only vary between $1.3\mu_B$ and $1.8\mu_B$.

TABLE I. Wave vectors $\mathbf{q}_1=(0,0,q)2\pi/a$ and $\mathbf{q}_2=(w,0,1)2\pi/a$ yielding the lowest energy between Γ and X and X and W, respectively. The energy minima are found through interpolation of the energy vs wave vector curves in Fig. 2.

Lattice parameter (a.u.)	q	$E(\mathbf{q}_1)$ (mRy)	w	$E(\mathbf{q}_2)$ (mRy)
6.82	0.53	−2.84	0.25	−1.09
6.78	0.54	−3.82	0.24	−2.45
6.74	0.54	−4.63	0.20	−3.65
6.70	0.55	−5.28	0.19	−4.61
6.66	0.55	−5.71	0.19	−5.30
6.60	0.59	−5.67	0.19	−5.69

From Fig. 2 we also see that a second minimum forms, on the $\overrightarrow{XW}$ symmetry line already for $a=6.78$ a.u. The new SS becomes the global minimum at $a=6.60$ a.u. with a $\mathbf{q}$ vector

$$\mathbf{q}_2=(w,0,1)\frac{2\pi}{a}. \tag{30}$$

Here w is close to 0.25 for the two largest volumes examined and around 0.19 for the remainder of the volumes; see Table I. This second SS state lies only around 0.3 mRy lower in energy than the AF state for all volumes considered.

It is very interesting to observe the almost degenerate energies in Fig. 2, for a large range of wave vectors between $\mathbf{q}_1$ and $\mathbf{q}_2$ for the case of $a=6.60$ a.u. This has occurred since the AF state gradually becomes closer in energy to the $\mathbf{q}_1$ SS.

Figure 3 shows the volume dependency of the energies for several magnetic structures, including the FM, AF, $\mathbf{q}_1$, and $\mathbf{q}_2$ orderings. Here we can observe that the transition from the $\mathbf{q}_1$ state to that of $\mathbf{q}_2$ takes place for a lattice constant $a=6.60$ a.u. and that the global energy minimum is almost degenerate between the two SS within the accuracy of our calculations. The $\mathbf{q}_1$ SS has its lowest energy at a lattice constant $a=6.63$ a.u. yielding $E(\mathbf{q}_1)=-5.79$ mRy below the reference energy, which should be compared to $E(\mathbf{q}_2)=-5.70$ mRy at $a=6.61$ a.u. The magnetization density of the former solution is displayed in Fig. 1.

Ideally, one ought to investigate the full irreducible wedge of the BZ, in order to determine the most stable SS. However, this would be too computational demanding. Instead, we have looked at whether the minima found along the $\overrightarrow{\Gamma X}$ and $\overrightarrow{XW}$ symmetry lines are local minima or merely saddle points. This requires calculations along one and two perpendicular directions around $\mathbf{q}_1$ and $\mathbf{q}_2$, respectively. Those calculations resulted in higher energies, confirming that both $\mathbf{q}_1$ and $\mathbf{q}_2$ are truly local minima.

C. 2k and 3k orderings

The type-I AF ordering in Sec. III B is also referred to as a $1\mathbf{k}$ structure, as it only involves *one* AF ordering vector. There are also the more complicated $2\mathbf{k}$ and $3\mathbf{k}$ structures,

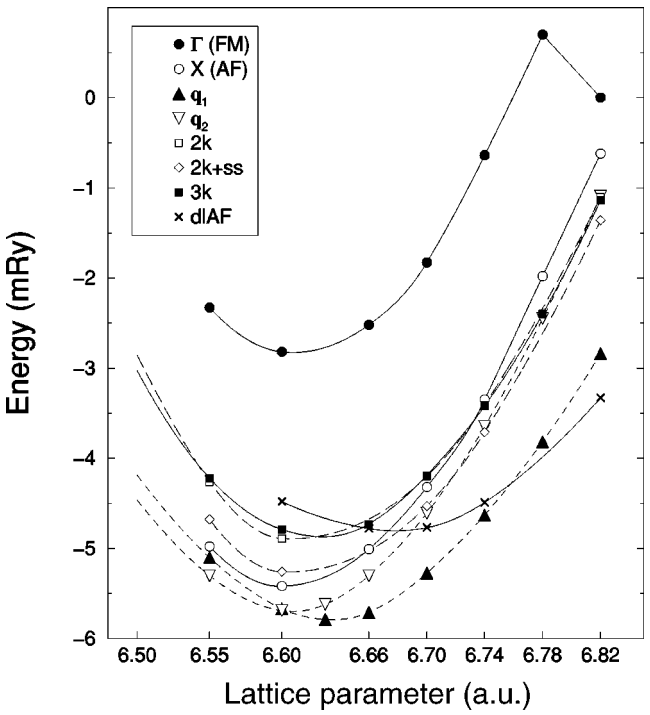

FIG. 3. Total energies vs volume, relative to the energy of the FM structure at $a=6.82$ a.u., for eight different orderings of the magnetic moments. The energies presented for the $\mathbf{q}_1$, $\mathbf{q}_2$, and $2\mathbf{k}$+ss structures are the (local) minimum energies with respect to the ordering vector for each lattice constant. The most stable orderings are in order of decreasing volume: the double-layered AF ordering ($a\geq 6.76$ a.u.), the spin spiral of wave vector $\mathbf{q}_1$ ($6.60<a<6.76$ a.u.), and finally the spin spiral of wave vector $\mathbf{q}_2$ ($a\leq 6.60$ a.u.). The lowest energy is almost degenerate between the two spin spirals, giving equilibrium volumes $a=6.63$ a.u. and $a=6.61$ a.u., respectively.

involving two and three independent AF $\mathbf{q}$ vectors, respectively. We have investigated these commensurate structures for the cases when

$$\mathbf{m}_{2\mathbf{k}}(\mathbf{r})=m(\mathbf{r})(e^{i\mathbf{q}_x\cdot\mathbf{r}},e^{i\mathbf{q}_y\cdot\mathbf{r}},0),$$

$$\mathbf{m}_{3\mathbf{k}}(\mathbf{r})=m(\mathbf{r})(e^{i\mathbf{q}_x\cdot\mathbf{r}},e^{i\mathbf{q}_y\cdot\mathbf{r}},e^{i\mathbf{q}_z\cdot\mathbf{r}}). \tag{31}$$

The $\mathbf{q}$ vectors point at X in the x, y, or z direction, according to their subscripts. The resulting magnetic structures are illustrated in Fig. 4, seen from the (001) surfaces of the conventional fcc cells. In the Heisenberg model, considering nearest-neighbor interaction only, these three AF structures ($1\mathbf{k}$, $2\mathbf{k}$, and $3\mathbf{k}$) are degenerate in energy.

The total energy curves in Fig. 3 show how the $2\mathbf{k}$ and $3\mathbf{k}$ structures are almost degenerate in energy for all volumes, while the $1\mathbf{k}$ (AF) energy crosses their energies around $a=6.73$ a.u., ending up considerably lower for volumes close to the equilibrium volume.

One can also add a SS to the $2\mathbf{k}$ structure, propagating along z so that the $\mathbf{q}$ vector rotates the $2\mathbf{k}$ ordered (001) planes relative to each other. This combined structure is interesting, since the experimental neutron scattering results[1]

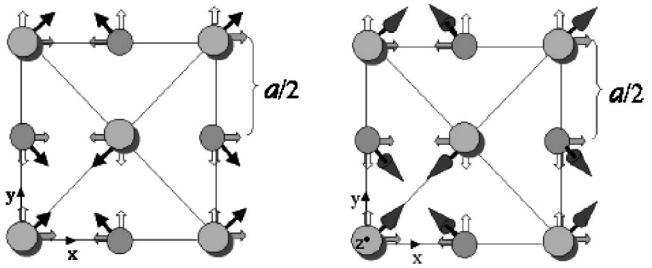

FIG. 4. Top views of the conventional fcc cell, showing the directions of the moments as in the $2\mathbf{k}$ (left picture) and $3\mathbf{k}$ (right picture) structures as black arrows. The gray and white arrows show the x and y components of the moments, respectively.

would not distinguish between that ordering of the moments and a pure SS ordering with $\mathbf{q}$ vector along $\overrightarrow{XW}$.

It is seen in Fig. 5 that the $2\mathbf{k}$ energy *is* lowered by the spin spiral, but only by 0.4 mRy/atom at most. This is for the smallest volume examined and yields a $\mathbf{q}$ vector

$$\mathbf{q}_3 = (0.16,0,1)\frac{2\pi}{a}, \tag{32}$$

thus an ordering vector that lies very close to the one found experimentally.

D. Double-layered antiferromagnetism

The fact that theoretical calculations in general give a very stable energy minimum for ordering vectors around $\mathbf{q}_1$ could be an indication of an even more stable double-layered type-I AF (dlAF) state, which corresponds to a commensurate longitudinal, instead of helical, spin density wave. Our

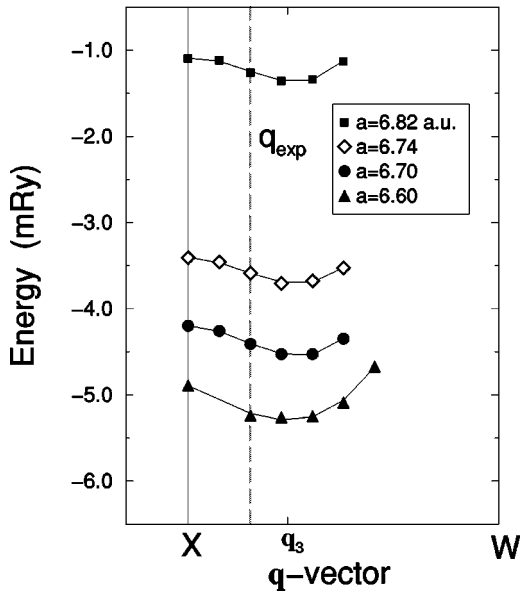

FIG. 5. Total energy as a function of the wave vector for a spin spiral on top of the $2\mathbf{k}$ structure. The total energies are given relative to the FM structure at $a=6.82$ a.u., and the lowest energy is found for the ordering vector $\mathbf{q}_3$ at $a=6.60$ a.u. This wave vector lies close to the experimental wave vector, indicated by the vertical dashed line.

results for this collinear structure show that this is true only for $a \geqslant 6.76$ a.u. (see Fig. 3), where the dlAF structure indeed has the lowest energy of the structures considered. This means that at the lattice constant of Cu, the dlAF state is the most stable structure among the here considered. However, the energy of the $\mathbf{q}_1$ SS lies considerably below that of the dlAF structure around the equilibrium volume.

IV. DISCUSSION

First, we observe that our energies corresponding to collinear structures in Fig. 3 are in very good agreement with earlier *collinear* FLAPW calculations using the GGA.[7] This is crucial and shows that our noncollinear implementation is correct. Both calculations find the dlAF ordering to be the most stable structure at $a=6.82$ a.u., lying 3 mRy below the AF state. The equilibrium volumes of the AF and dlAF structures in Fig. 3 are identical to those in Ref. 7, although we do not find the energies to be degenerate. Instead they differ by around 0.6 mRy, a difference probably hidden in the coarser energy resolution of the earlier calculation.

Taking noncollinear structures into account, we find a transition from the dlAF structure to the $\mathbf{q}_1$ SS at $a=6.76$ a.u., which stays lowest in energy for smaller lattice constants. The same general trend, a dlAF structure changing into a more complex noncollinear ordering as the volume decreases, has been found also in some ASA calculations.[4,5] Using the LSDA, Antropov *et al.*[4] found their dlAF structure to change into a $3\mathbf{k}$ ordering for $a<6.78$ a.u., while in their GGA calculations the dlAF structure was followed by a noncollinear configuration described in an eight-atom unitcell. The transition occurred around $a=6.69$ a.u., and the new noncollinear structure could be viewed as a slightly distorted $\mathbf{q}_1$ SS. In fact, the eight-atom structure and the SS were nearly degenerated for $a>6.60$ a.u. and identical for $a<6.60$ a.u., since the distortion then had disappeared. Antropov *et al.*[4] also compared two different LMTO basis sets for their GGA calculations, using the ASA with the ''combined correction'' term. The first basis set includes only spd orbitals, while the second has additional f orbitals. The outcomes of the two calculations are very different (cf. Fig. 2 and Fig. 6 in Ref. 4), and only those of the latter are consistent with our results. The LSDA calculations by James *et al.*,[5] using the LMTO-ASA method, without the ''combined correction'' term and with spd orbitals in the basis set, show a trend in line with our results. However, they find a stable $3\mathbf{k}$ structure for $a<6.78$ a.u., in accordance with the LSDA results of Antropov *et al.* Thus, it seems that while the LSDA stabilizes a $3\mathbf{k}$ structure for intermediate volumes, the GGA calculations prefer a SS.

All calculations show a crossover from a HS to a LS state for the ferromagnetic solution. The corresponding transition volume in Fig. 3 (just below $a=6.78$ a.u.) is in excellent agreement with the full-potential calculations of Ref. 7. The ASA calculations show a fairly large spread for this transition. In the calculations by Mryasov *et al.*,[2] the HS-LS crossover is found at a larger lattice constant, giving a LS solution even for $a=6.80$ a.u., while Antropov *et al.*[4] find the crossover already at $a=6.71$ a.u. The calculations by James

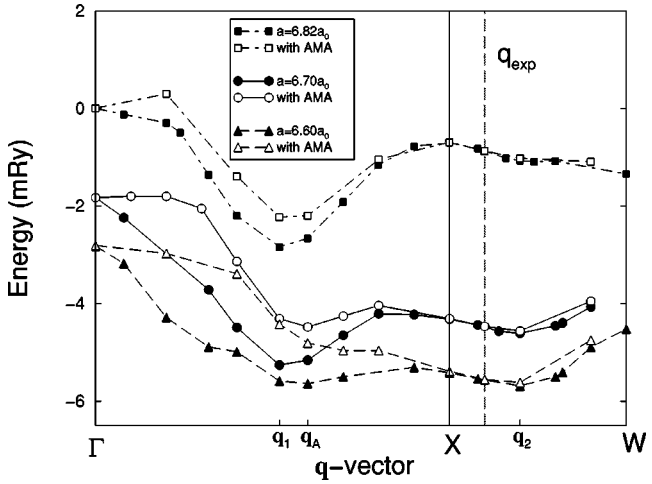

FIG. 6. Comparing the atomic moment approximation with a full vector treatment of the magnetic moments for three different volumes. The energies from Γ to X are largely effected by the approximation, shifting the stable SS towards X.

et al.[5] show a transition around $a=6.78$ a.u. in agreement with our findings.

However, although the ASA calculations show the correct overall trend regarding the volume dependence of the magnetic structures, there are some systematic errors in the energies as shown by Körling and Ergon.[6] This is maybe most clearly displayed in the spin-spiral calculations. Comparing to other SS calculations, our results confirm a stable SS almost halfway from Γ to X. Here it can be noted that we, in accordance with other methods using a vector field treatment of the magnetic moments,[8,11] i.e., beyond the AMA, find a wave vector closer to $\mathbf{q}=(0,0,0.55)$ for $a>6.60$ a.u., as compared to the the AMA calculations[2,3,6,12] where the most stable wave vector is found closer to X, at $\mathbf{q}_A$ defined in Sec. I.

In order to study this effect we have performed forced AMA [see Eq. (13)] calculations for three different volumes. In Fig. 6 it is clearly seen how the energies along the $\overrightarrow{\Gamma X}$ direction are the most sensitive to restrictions of the noncollinearity inside the MT spheres. The energies of the $\mathbf{q}_1$ SS state in the AMA are approximately 1 mRy higher than in the full field calculations for the two smaller volumes, and the stable SS is therefore shifted from $\mathbf{q}_1$ to $\mathbf{q}_A$. Further, the $\mathbf{q}_2$ SS is stabilized already for $a=6.70$ a.u. in the AMA calculations.

Now, if one studies the unconstrained magnetization density in Fig. 1, it is possible to observe that it is fairly collinear closer to the atomic sites and the rotations occur mainly in-between the atoms. However, these rotations may be significant already inside the muffin-tin spheres, which in Fig. 1, if displayed, would be almost touching circles centered around the nine atomic centra.

Kurz *et al.*[12] uses the same kind of AMA as we did above, with fixed directions within each muffin-tin sphere but full freedom in between, in their LAPW study of spin spirals for $a=6.70$ a.u. Unlike our results in Fig. 6, their most stable SS at this volume has the ordering vector $\mathbf{q}_A$, which might be an effect of a smaller plane-wave cutoff. However, their AMA calculations confirm our AMA increase in energy for $\mathbf{q}$ vectors close to Γ.

Interesting SS results are found along the $\overrightarrow{XW}$ symmetry line. The eager search for $\mathbf{q}_{expt}$ has led to a number of different results for this region in earlier calculations. We reproduce the SS of $\mathbf{q}_B=W$ found in Ref. 6, only as a local minimum for the largest volume. Apart from the stabilization of $\mathbf{q}_2$ at $a=6.60$ a.u., it is highly interesting to see the remarkable flattening of the energy curve. Together with a change in moments from almost $1.5\mu_B$ down to $1.2\mu_B$ for $\mathbf{q}$ vectors between $\mathbf{q}_1$ and $\mathbf{q}_2$, this opens the possibility of the coexistence of a number of noncollinear structures with varying sizes of the magnetic moments. The flat energy curve could also explain why the MASW (Ref. 11), calculation finds a wave vector $\mathbf{q}_C$ slightly different from $\mathbf{q}_2$, since the results in this region are probably very sensitive to any modification of the potential. It should be noted, however, that Knöpfle *et al.* find $\mathbf{q}_C$ to be stable already at $a=6.70$ a.u.

The $2\mathbf{k}$ structure in combination with a SS yields the lowest energy for $\mathbf{q}_3$, close to the experimental wave vector.[1] It is therefore very tempting to believe that this is the magnetic structure they observed in the experiment, although the volume is much smaller than what they claim to have in the experiments. Further, the energy of this structure lies 0.4 mRy above the global energy minimum in Fig. 3.

V. CONCLUSIONS

We have presented a noncollinear implementation into a full-potential linearized augmented-plane-wave method. According to our FP-APW+lo calculations for γ-Fe, using the GGA and investigating a number of collinear as well as noncollinear magnetic orderings, the double-layered AF structure has the lowest energy for the largest lattice constant considered, equivalent to that of copper ($a=6.82$ a.u.), while the ground state consists of a set of almost degenerate spin-spiral states (around $a=6.61$–6.63 a.u.).

The stable magnetic structure is very sensitive to volume changes, and the dlAF is stable for lattice constants down to $a=6.76$ a.u., where a SS structure becomes lower in energy. This SS, in turn, changes the ordering vector from $\mathbf{q}_1$ to $\mathbf{q}_2$ for volumes with $a<6.60$ a.u. From our results together with earlier calculations,[4,5] one can conclude that while the GGA stabilizes a SS structure at smaller volumes, the LSDA seems to predict the $3\mathbf{k}$ to be lowest in energy. Calculations are in progress to verify if this is the case also for the LSDA with an unconstrained vector representation of the magnetization density.

At $a=6.60$ a.u. there is a continuum of $\mathbf{q}$ vectors between $\mathbf{q}_1$ and $\mathbf{q}_2$ being almost degenerate in energy. This flattening of the energy curve is not seen within the AMA (see Fig. 6), since the energies in the $\overrightarrow{\Gamma X}$ direction are dramatically altered by the restriction of the noncollinearity within each MT sphere.

The $2\mathbf{k}$ and $3\mathbf{k}$ structures have quite high energies for all examined volumes. However, a SS of wave vector $\mathbf{q}_3=(0.16,0,1)2\pi/a$ superimposed on the $2\mathbf{k}$ structure at $a=6.60$ a.u. lowers the energy to only 0.4 mRy above the

global energy minimum. This structure, as well as the $\mathbf{q}_2$ SS, is compatible with the reported experimental results,[1] but it becomes stable only at volumes much smaller than the volume which is claimed to be the experimental. Hence, one has to conclude that state-of-the-art density functional calculations fail to reproduce the experimental magnetic structure for fcc Fe at the lattice constant of Cu.

Finally, the lowest energy of all structures and all volumes examined in the present work, were found to be almost degenerate between the $\mathbf{q}_1$ and the $\mathbf{q}_2$ SS. The first SS has an equilibrium volume of $a=6.63$ a.u. and lies 5.79 mRy below the reference energy (the energy of the FM structure at $a=6.82$ a.u.). The latter SS has its energy minimum at $a=6.61$ a.u., 5.70 mRy below the reference energy. These two states can, with the present computational accuracy, be considered to be degenerate, and around this equilibrium volume there is actually a nearly degenerate continuum of SS states between $\mathbf{q}_1$ and $\mathbf{q}_2$. This is very interesting, since this situation with many different magnetic structures close in energy is related to what has been found and used to explain the Invar effect for the alloy fcc $Fe_{0.65}Ni_{0.35}$.[32]

ACKNOWLEDGMENTS

The authors are thankful for discussions with Dr. Igor Abrikosov, Dr. Leonid Sandratskii, and Dr. David Singh. Support from the Swedish Research Council (VR) and the Swedish Strategic Research Foundation (SSF) is acknowledged. Part of the calculations have been performed at the Swedish National Supercomputer Center in Linköping (NSC).

[1] Y. Tsunoda, J. Phys.: Condens. Matter **1**, 10 427 (1989).
[2] O. N. Mryasov, A. I. Liechtenstein, L. M. Sandratskii, and V. A. Gubanov, J. Phys.: Condens. Matter **3**, 7683 (1991).
[3] M. Uhl, L. M. Sandratskii, and J. Kübler, J. Magn. Magn. Mater. **103**, 314 (1992).
[4] V. P. Antropov, M. I. Katsnelson, M. van Schilfgaarde, and B. Harmon, Phys. Rev. Lett. **75**, 729 (1995); V. P. Antropov, M. I. Katsnelson, B. Harmon, M. van Schilfgaarde, and D. Kusnezov, Phys. Rev. B **54**, 1019 (1996).
[5] P. James, O. Eriksson, B. Johansson, and I. A. Abrikosov, Phys. Rev. B **59**, 419 (1999).
[6] M. Körling and J. Ergon, Phys. Rev. B **54**, 8293 (1996).
[7] H. C. Herper, E. Hoffmann, and P. Entel, Phys. Rev. B **60**, 3839 (1999).
[8] D. M. Bylander and L. Kleinman, Phys. Rev. B **58**, 9207 (1998).
[9] D. M. Bylander and L. Kleinman, Phys. Rev. B **59**, 6278 (1999).
[10] D. M. Bylander and L. Kleinman, Phys. Rev. B **60**, 9916 (1999).
[11] K. Knöpfle, L. M. Sandratskii, and J. Kübler, Phys. Rev. B **62**, 5564 (2000).
[12] Ph. Kurz, F. Förster, L. Nordström, G. Bihlmayer, and S. Blügel (unpublished).
[13] L. Nordström and D. J. Singh, Phys. Rev. Lett. **76**, 4420 (1996).
[14] P. H. Andersson, L. Nordström, and O. Eriksson, Phys. Rev. B **60**, 6765 (1999).
[15] L. Nordström and A. Mavromaras, Europhys. Lett. **49**, 775 (2000).
[16] J. Kübler, K.-H. Höck, J. Sticht, and A. R. Williams, J. Phys. F: Met. Phys. **18**, 469 (1988).
[17] L. M. Sandratskii and P. G. Guletskii, J. Phys. F: Met. Phys. **16**, 43 (1986).
[18] U. von Barth and L. Hedin, J. Phys. C **5**, 1629 (1972).
[19] E. Sjöstedt, L. Nordström, and D. J. Singh, Solid State Commun. **114**, 15 (2000).
[20] P. Hohenberg and W. Kohn, Phys. Rev. **136**, B864 (1964).
[21] W. Kohn and L. J. Sham, Phys. Rev. **140**, A1133 (1965).
[22] D. M. Ceperley and B. J. Alder, Phys. Rev. Lett. **45**, 566 (1980).
[23] S. H. Vosko, L. Wilk, and M. Nusair, Can. J. Phys. **58**, 1200 (1980).
[24] J. P. Perdew and Y. Wang, Phys. Rev. B **45**, 13 244 (1992).
[25] J. P. Perdew, K. Burke, and M. Ernzerhof, Phys. Rev. Lett. **77**, 3865 (1996).
[26] K. Capelle and E. K. U. Gross, Phys. Rev. Lett. **78**, 1872 (1997).
[27] Although seeming natural, this is not always the best choice of AMA quantization axis, as discussed in O. Grotheer, C. Ederer, and M. Fähnle, Phys. Rev. B **62**, 5601 (2000).
[28] O. K. Andersen, Phys. Rev. B **12**, 3060 (1975).
[29] D. J. Singh, *Planewaves, Pseudopotentials and the LAPW Method* (Kluwer Academic, Boston, 1994) and references therein.
[30] D. J. Singh, Phys. Rev. B **43**, 6388 (1991).
[31] C. Herring, in *Magnetism*, edited by G. T. Rado and H. Suhl (Academic Press, New York, 1966), Vol. 4.
[32] M. van Schilfgaarde, I. A. Abrikosov, and B. Johansson, Nature (London) **400**, 46 (1999).